Journal of Inflammation Research

Dovepress
open access to scientific and medical research

Open Access Full Text Article

ORIGINAL RESEARCH

Metabolomic Profiling of Lungs from Mice Reveals the Variability of Metabolites in *Pneumocystis* Infection and the Metabolic Abnormalities in BAFF-R-Deficient Mice

Heng-Mo Rong*, Han-Yu-Jie Kang*, Zhao-Hui Tong

Department of Respiratory and Critical Care Medicine, Beijing Institute of Respiratory Medicine, Beijing Chao-Yang Hospital, Capital Medical University, Beijing, 100020, People's Republic of China

*These authors contributed equally to this work

Correspondence: Zhao-Hui Tong, Department of Respiratory and Critical Care Medicine, Beijing Institute of Respiratory Medicine, Beijing Chao-yang Hospital, Capital Medical University, NO. 8, Gong Ti South Road, Chao yang District, Beijing, 100020, People's Republic of China, Tel +86 13910930309, Email tongzhaohuicy@sina.com

Purpose: The incidence of *Pneumocystis* pneumonia (PCP) in patients without human immunodeficiency virus (HIV) has been increasing. In this study, we aimed to investigate the metabolic changes in *Pneumocystis* infection and the metabolic abnormalities in B-cell-activating factor receptor (BAFF-R)-deficient mice with *Pneumocystis* infection.

Methods: The important function of B cells during *Pneumocystis* infection is increasingly recognized. In this study, a *Pneumocystis*-infected mouse model was constructed in BAFF-R$^{-/-}$ mice and wild-type (WT) mice. Lungs of uninfected WT C57BL/6, WT *Pneumocystis*-infected, and BAFF-R$^{-/-}$ *Pneumocystis*-infected mice were used for metabolomic analyses to compare the metabolomic profiles among the groups, with the aim of exploring the metabolic influence of *Pneumocystis* infection and the influence of mature B-cell deficiency during infection.

Results: The results indicated that many metabolites, mainly lipids and lipid-like molecules, were dysregulated in *Pneumocystis*-infected WT mice compared with uninfected WT C57BL/6 mice. The data also demonstrated significant changes in tryptophan metabolism, and the expression levels of key enzymes of tryptophan metabolism, such as indoleamine 2,3-dioxygenase 1 (IDO1), were significantly upregulated. In addition, B-cell development and function might be associated with lipid metabolism. We found a lower level of alitretinoin and the abnormalities of fatty acid metabolism in BAFF-R$^{-/-}$ *Pneumocystis*-infected mice. The mRNA levels of enzymes associated with fatty acid metabolism in the lung were upregulated in BAFF-R$^{-/-}$ *Pneumocystis*-infected mice and positively correlated with the level of IL17A, thus suggesting that the abnormalities of fatty acid metabolism may be associated with greater inflammatory cell infiltration in the lung tissue of BAFF-R$^{-/-}$ *Pneumocystis*-infected mice compared with the WT *Pneumocystis*-infected mice.

Conclusion: Our data revealed the variability of metabolites in *Pneumocystis*-infected mice, suggesting that the metabolism plays a vital role in the immune response to *Pneumocystis* infection.

Keywords: *Pneumocystis* pneumonia, metabolomics, B lymphocytes, inflammation

Introduction

Pneumocystis pneumonia (PCP) is a life-threatening complication in immunosuppressed subjects without human immunodeficiency virus (HIV).[1] Given the increase in organ transplantation and the widespread use of immunosuppressive drugs, the incidence of PCP in the non-HIV immunocompromised population has been rising.[2] Intensive care unit (ICU) admission, mechanical ventilation rates, and mortality are higher in HIV-negative patients than in HIV-positive patients after PCP infection.[3,4] Thus, it is necessary to better understand the immune mechanism of HIV-negative PCP and explore new therapeutic targets to improve the current treatment.

Received: 24 October 2022
Accepted: 14 March 2023
Published: 27 March 2023

$CD4^+$ T cells play a crucial role in the immune response to *Pneumocystis* by recruiting effector cells to the lungs.[5] Previous studies have shown that the loss of $CD4^+$ T cells makes the murine susceptible to *Pneumocystis* infection.[6,7] Many studies have demonstrated that diverse $CD4^+$ T-cell subsets, such as Th1 cells and Th17 cells, are induced after *Pneumocystis* infection.[8–10] In addition, there is growing evidence that B cells are also crucial in the immune response against *Pneumocystis* infection.[11,12] B cells are responsible for antibody production and antigen presentation.[12] According to studies in murine models, anti-CD20 antibody therapy makes mice susceptible to *Pneumocystis* pneumonia.[13] In addition to the generation of *Pneumocystis*-specific antibodies, B cells are also crucial for priming $CD4^+$ T cells for the clearance of *Pneumocystis*.[14] Overall, previous studies have indicated that B cells are both effector cells and responsible for priming $CD4^+$ T cells.[11]

As for B cells, our previous studies have suggested that corticosteroid-treated hosts with PCP have apparent suppression in B cells immunity, which emphasizes the importance of B cells in the anti-*Pneumocystis* defense.[15] In addition, we used B-cell-activating factor receptor-deficient mice (BAFF-$R^{-/-}$ mice) to explore the B-cell-mediated function in *Pneumocystis* infection. B-cell-activating factor (BAFF) —a member of the tumor necrosis factor (TNF) family—is fundamental for the survival of B cells.[16] BAFF receptor (BAFF-R) is the receptor for BAFF and is the key for BAFF-mediated mature B- cell survival,[17] which means that BAFF-R deficiency results in B-cell maturation disorders. Our previous research evaluated the role of BAFF-R in host defense against *Pneumocystis* and showed that the percentages of mature B cells, naïve B cells, and functional B cells expressing IgM and IgD antibodies in the lung and blood declined in BAFF-$R^{-/-}$ mice compared with wild-type (WT) mice infected with *Pneumocystis* at 2 weeks. BAFF-R deficiency also resulted in impaired production of *Pneumocystis*-specific antibodies, delayed clearance of *Pneumocystis*, and more significant inflammatory cell infiltration of the lungs in BAFF-$R^{-/-}$ mice, although no significant respiratory distress was seen in *Pneumocystis*-infected WT mice and BAFF-R-deficient mice, and there was no significant difference in body weight between the groups;[18] however, the mechanism still needs to be further explored.

Recent studies have shown that metabolism plays a critical role in regulating the function of immune cells.[19,20] In infectious diseases, metabolism is also important in the body's immune defense to prevent pathogens. For example, a previous study showed that increased glycolysis could enhance the effector function of $CD8^+$ T cells in HIV infection.[21] In SARS-CoV-2 infection, it has been found that enhanced B-cell metabolism after illness leads to the downregulation of CD19 expression in B cells, resulting in immunodeficiency in recovered patients.[22] Untargeted metabolomics is a commonly used method. This method can detect all of the measurable metabolites in a sample to help understand the current body state.[23] Several recent studies have shown significant changes in serum metabolic composition in COVID-19 patients compared with healthy individuals, and these changes are associated with disease severity.[24–26] However, the metabolic changes in PCP remain unclear.

In this study, we performed metabolomic analysis to explore the effects of *Pneumocystis* infection on metabolic profiles so as to develop new potential therapeutic targets. In addition, to further explore the role of mature B cells in *Pneumocystis* infection, we performed a metabolomic analysis of mouse lung tissues to compare the metabolomic profiles between WT *Pneumocystis*-infected mice and BAFF-$R^{-/-}$ *Pneumocystis*-infected mice so as to reveal the effects of mature B-cell deficiency on metabolism.

Materials and Methods

Mice

WT C57BL/6 mice and severe combined immunodeficient (SCID) mice were purchased from Vital River Laboratory Animal Co., Ltd. (Beijing, China). BAFF-$R^{-/-}$ mice on a C57BL/6 background were obtained from The Jackson Laboratory (Bar Harbor, ME, USA). All of the mice used in this study were 6-8-week-old females. They were bred in specific pathogen-free conditions. The study was approved by the Capital Medical University Animal Care and Use Committee and followed the National Institutes of Health (NIH) Guide for the Care and Use of Laboratory Animals and the Guidelines for Chinese Regulation for the Use and Care of Laboratory Animals.

Pneumocystis Lung Infection

Pneumocystis murina was obtained from the American Type Culture Collection and maintained in SCID mice as previously described.[15,18] In brief, the lungs from SCID mice infected with *Pneumocystis murina* were homogenized and were pelleted at 1,000 *g* for 10 min at 4°C. Phosphate-buffered saline (PBS) was used to resuspend the pellet, and then the lung homogenates were stained by Diff Quick (Baxter, McGraw Park, IL). We microscopically determined the number of *Pneumocystis* cysts, which was adjusted to a concentration of 1×10^7 cysts/mL, and these were frozen to establish subsequent *Pneumocystis* infection models. The murine models of *Pneumocystis* infection were prepared by intratracheally inoculating with 1×10^6 *Pneumocystis* cysts diluted in 100 μL PBS. Control mice were intratracheally injected with lung homogenates from uninfected SCID mice.

Sample Preparation and Extraction for Untargeted Metabolomics

According to our prior study,[18] the most severe lung inflammation and the highest *Pneumocystis* load were observed at 2 weeks after infection. Thus, mouse lung tissues were collected at 2 weeks after *Pneumocystis* infection and stored at −80° C until use. The lung tissues were thawed on ice. The lung tissue (50 ± 2 mg) was homogenized with 500 μL of 70% methanol at 30 Hz for 3 min. After homogenization, the mixture was shaken for 5 min and incubated on ice for 15 min. Then, the mixture was centrifuged at 12,000 rpm for 10 min at 4° C, and 400 μL of the supernatant was collected in another tube. A total of 500 μL ethyl acetate/methanol was added into the precipitate of the centrifuge tube, and the mixture was oscillated for 5 min and incubated on ice for 15 min. Next, 400 μL of the supernatant was collected after centrifugation at 12,000 rpm for 10 min at 4°C. The two supernatants were merged and concentrated. Concentration was achieved using a freeze concentrator (7310038, LABCONCO, Thermo) at 4°C and 3000 r/min overnight. Then 100 μL of 70% methanol was added, and an ultrasound was performed for 3 min. After centrifugation at 12,000 rpm for 3 min at 4°C, 60 μL of the supernatant was collected for LC-MS analysis.

HPLC Conditions (T3)

All of the sample extracts were analyzed by the LC-MS system. The analytical conditions were as follows: UPLC: column, Waters ACQUITY UPLC HSS T3 C18 (1.8 μm, 2.1 mm × 100 mm); column temperature, 40°C; flow rate, 0.4 mL/min; injection volume, 2uL; solvent system, water (0.1% formic acid): acetonitrile (0.1% formic acid); gradient program, 95:5 V/V at 0 min, 10:90 V/V at 11.0 min, 10:90 V/V at 12.0 min, 95:5 V/V at 12.1 min, and 95:5 V/V at 14.0 min.

Identification of the Metabolic Information

The raw data obtained by LC-MS analysis were first converted into mzML format by ProteoWizard software. Peak extraction, alignment, and retention time correction were performed by the XCMS program. The SVR method was used to correct the peak area and filter the peaks with a loss rate > 50% in each group of samples. Then, the metabolic identification information was acquired by searching the laboratory's self-built database and integrating the public database and metDNA.

Real-Time PCR

RNAs were purified from the homogenized lung tissue by TRIzol reagent (Invitrogen Life Technologies, Carlsbad, CA, USA) and reverse-transcribed using the PrimeScript TM II 1st Strand cDNA Synthesis Kit (Takara Bio, Dalian, China). cDNA (1 μg) was used as template for RT-PCR, which was performed using SYBR PreMix Ex Taq TM II ROX plus (Takara) and the ABI Prism 7500 Sequence Detection System (Applied Biosystems, Foster City, CA). Gene expression was calculated using the $2^{-\Delta\Delta CT}$ method after normalization to β-actin (Actb). The Primers' sequences are listed in Supplemental Table 1.

Statistical Analysis

Statistical analysis was performed by the R program. The statistical significance was set at $p < 0.05$. Univariate statistical analysis included Student's *t*-test and variance multiple analysis. Multivariate statistical analysis included principal component analysis (PCA) and orthogonal partial least-squares discriminant analysis (OPLS-DA). PCA was performed by the base package in

R software (version 3.5.0). OPLS-DA of metabolomic data was performed by MetaboAnalystR (version 1.0.1) in R software (version 3.5.0). The significantly different metabolites between the groups were filtered and confirmed by combining the results of the variable importance in projection (VIP) values (VIP > 1.0), *t*-test ($P < 0.05$), and fold change (FC) values (FC ≥ 2.0 or FC ≤ 0.5). The significantly different metabolites were used for pathway analysis with the Kyoto Encyclopedia of Genes and Genomes biological pathway database, and metabolic pathways with $P < 0.05$ were defined as being significantly enriched.

Results

Metabolic Profiling of Lung Samples

For untargeted metabolomic analysis, lung samples were obtained from seven uninfected WT mice in the control group, seven WT *Pneumocystis*-infected mice, and seven BAFF-R$^{-/-}$ *Pneumocystis*-infected mice. PCA was used to investigate the degree of variation between the groups in both ion modes, and a grouping trend between the groups could be observed (Figure 1). Then, OPLS-DA was performed to further explore the differences between the groups in electrospray ionization positive (ESI +) and negative (ESI-) modes. As shown in Figure 2, a clearer separation between the groups was observed.

A total of 302 differential metabolites in the lungs were identified in the positive ion mode between control mice and WT *Pneumocystis*-infected mice. The levels of 73 metabolites were higher, whereas the levels of 229 metabolites were lower in the lungs of WT *Pneumocystis*-infected mice compared with control mice. In the negative ion mode, we

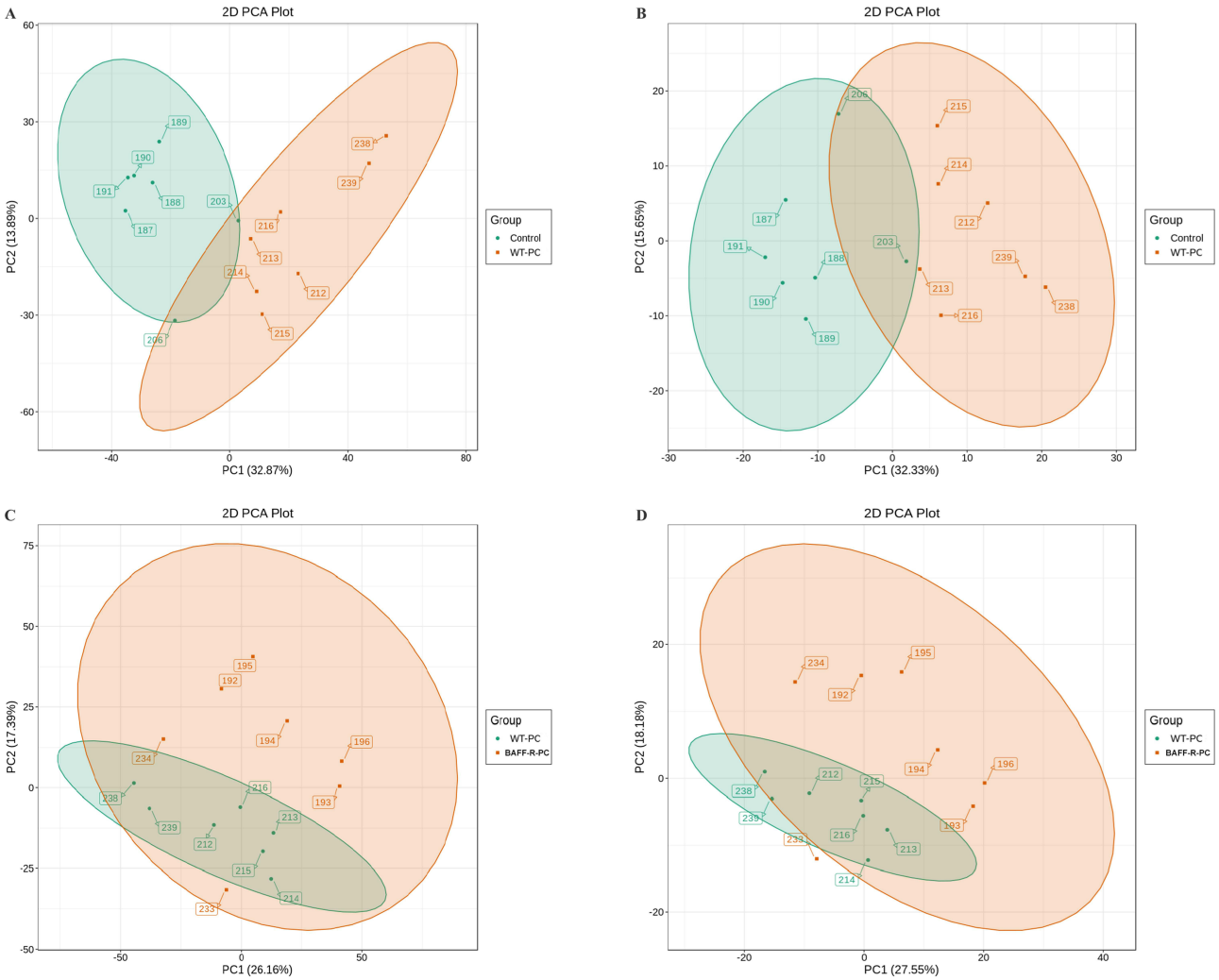

Figure 1 Scatter plot of scores based on the PCA model. (**A**) Positive ion (ESI^+) scan between the control group and *Pneumocystis*-infected wild-type (WT) mice; (**B**) Negative ion (ESI^-) scan between the control group and *Pneumocystis*-infected WT mice; (**C**) ESI^+ scan between the *Pneumocystis*-infected WT mice and *Pneumocystis*-infected BAFF-R$^{-/-}$ mice; (**D**) ESI^- scan between the *Pneumocystis*-infected WT mice and *Pneumocystis*-infected BAFF-R$^{-/-}$ mice.

detected 66 differential metabolites between the control group and the WT *Pneumocystis*-infected group, of which 21 metabolites were upregulated and 45 metabolites were downregulated. The details are shown in Supplemental Tables 2, 3, and Figure 3. Heatmaps presented a different pattern of metabolites between the control and WT *Pneumocystis*-infected mice in both the positive and negative ion modes (Supplemental Figures 1 and 2).

In the comparison between WT *Pneumocystis*-infected mice and BAFF-R$^{-/-}$ *Pneumocystis*-infected mice, 105 differential metabolites were identified in the lung samples, of which 85 were found in the positive ion mode and 23 in the negative ion mode. The results are summarized in Supplemental Tables 4 and 5. In the positive ion mode, 44 metabolites were upregulated and 41 metabolites were downregulated in the lungs of BAFF-R$^{-/-}$ *Pneumocystis*-infected mice compared with WT *Pneumocystis*-infected mice. In the negative ion mode, seven metabolites were upregulated and 16 metabolites were downregulated. A volcano plot is shown in Figure 4. Heatmaps showed differential metabolic profiles of lung samples between WT *Pneumocystis*-infected mice and BAFF-R$^{-/-}$ *Pneumocystis*-infected mice (Supplemental Figures 3 and 4).

Dysregulated Lipids and Lipid-Like Molecules and Significant Changes in Products from Tryptophan Metabolism in WT *Pneumocystis*-Infected Mice

The significantly dysregulated metabolites included lipids and lipid-like molecules, amino acid and its metabolomics, and organic acids and derivatives (Table 1). The findings are consistent with those of other studies on

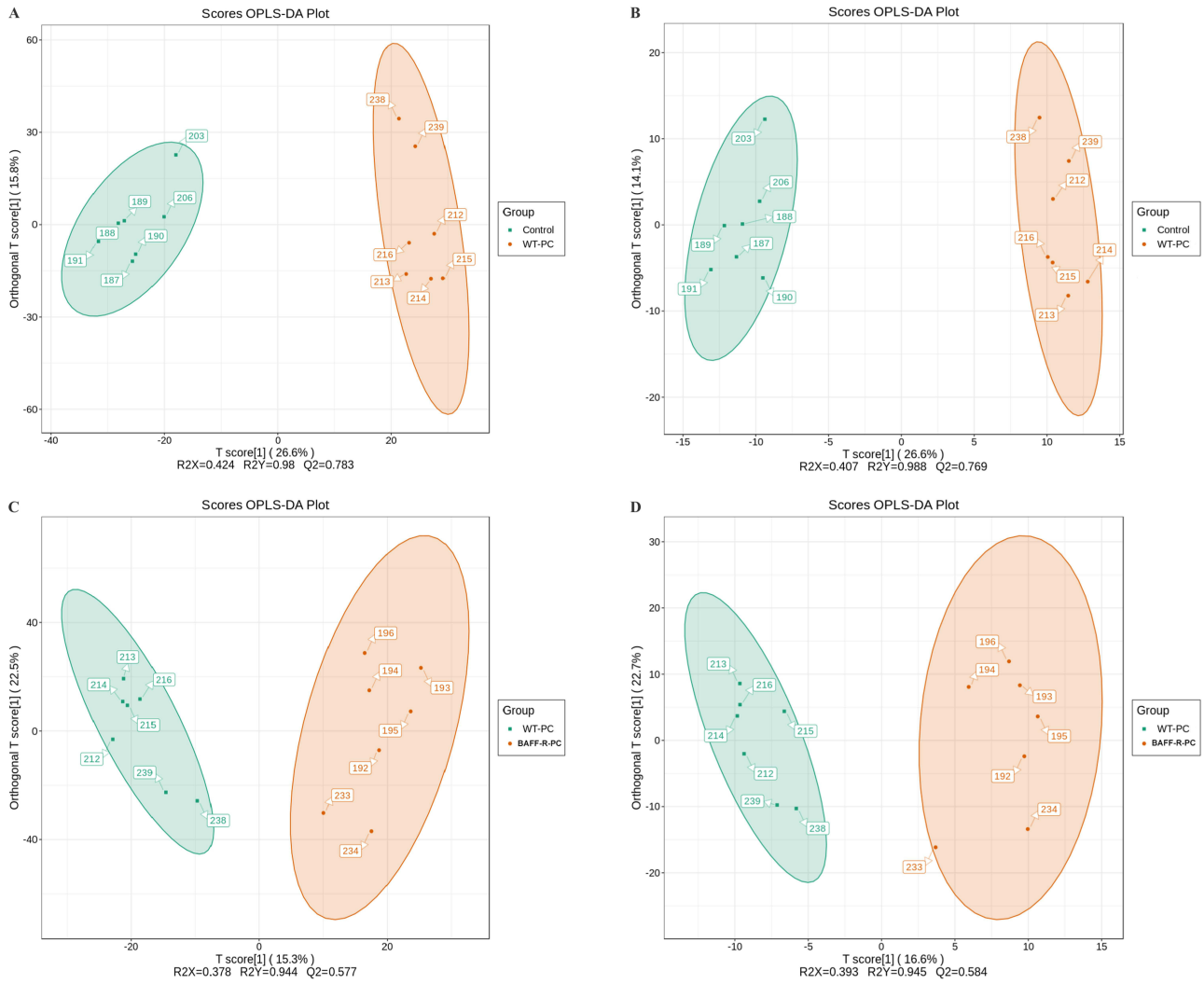

Figure 2 Scatter plot of scores based on the OPLS-DA model. (**A**) ESI$^+$ scan between the control group and *Pneumocystis*-infected WT mice; (**B**) ESI$^-$ scan between the control group and *Pneumocystis*-infected WT mice; (**C**) ESI$^+$ scan between the *Pneumocystis*-infected WT mice and *Pneumocystis*-infected BAFF-R$^{-/-}$ mice; (**D**) ESI$^-$ scan between the *Pneumocystis*-infected WT mice and *Pneumocystis*-infected BAFF-R$^{-/-}$ mice.

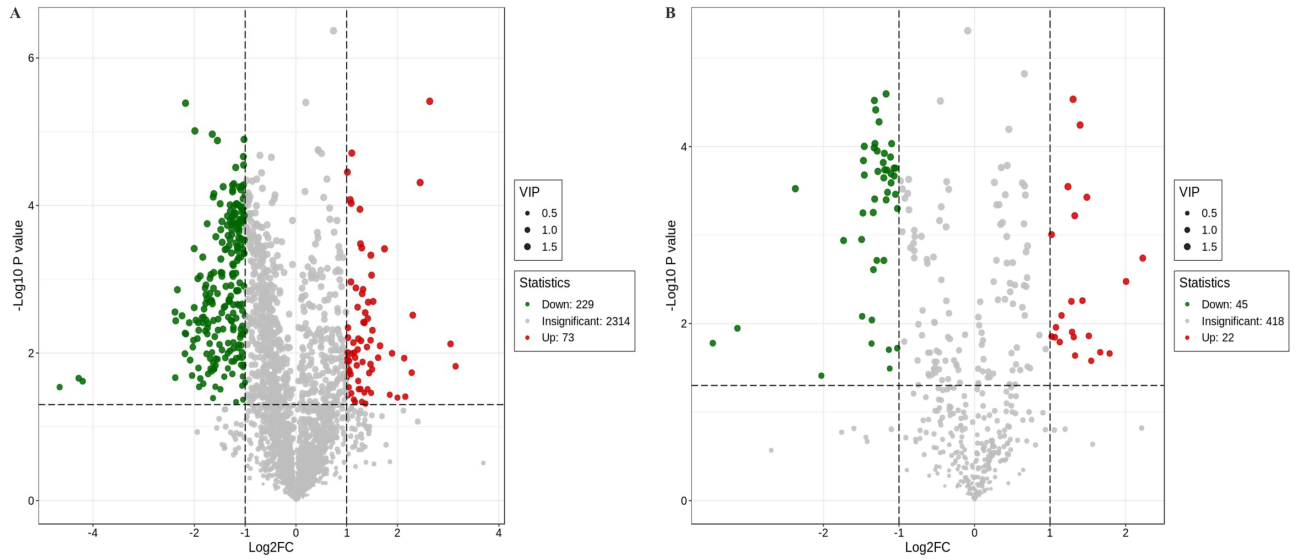

Figure 3 Volcano plot showing the number and distribution of lung metabolites in the control group and *Pneumocystis*-infected WT mice. (**A**) Positive and (**B**) negative ion modes.

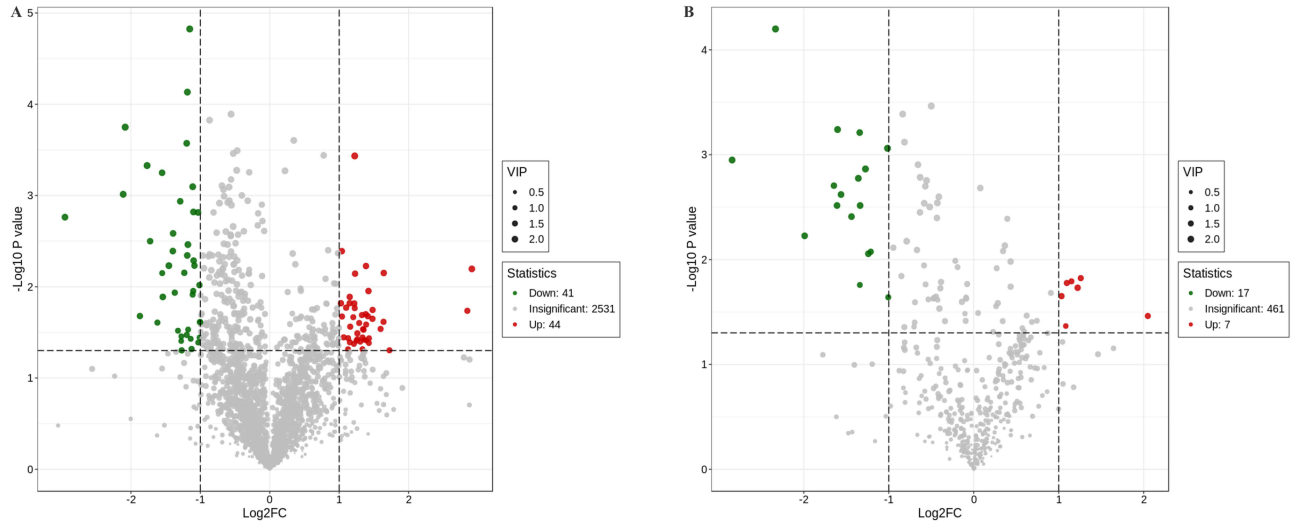

Figure 4 Volcano plot showing the number and distribution of lung metabolites in the *Pneumocystis*-infected WT mice and *Pneumocystis*-infected BAFF-R$^{-/-}$ mice. (**A**) Positive and (**B**) negative ion modes.

patients with ventilator-associated pneumonia (VAP) or community-acquired pneumonia (CAP).[27,28] Most of the differential metabolites exhibited downregulation in WT *Pneumocystis*-infected mice, such as PA (21:0/i-15:0), TG (18:2 (9Z,12Z)/20:5 (5Z,8Z,11Z,14Z,17Z)/18:4 (6Z,9Z,12Z,15Z)), PA (i-21:0/a-15:0), medroxyprogesterone 17-acetate, methylprednisolone succinate, PE-NMe2 (20:5 (5Z,8Z,11Z,14Z,17Z)/22:6 (4Z,7Z,10Z,13Z,16Z,19Z)), P-aminohippuric acid, 2-amino-3-(3-methylbut-2-enylthio) propionic acid, and raltitrexed (Supplemental Figure 5). However, some lipids and lipid-like molecules, such as PC (14:0/22:2 (13Z,16Z)), DG (22:1 (13Z)/20:5 (5Z,8Z,11Z,14Z,17Z)/0:0), and cis-7,10,13,16,19-docosapentaenoic acid, were upregulated (Supplemental Figure 5) in WT *Pneumocystis*-infected mice. The top 20 differential metabolites between the control group and the *Pneumocystis*-infected WT group with the highest VIP values under ESI- and ESI+ modes are presented in Table 1.

Table 1 Top 20 Differential Metabolites Between the Control Group and *Pneumocystis*-Infected WT Group with the Highest VIP Values Under ESI- and ESI+ Modes

Positive ion (ESI+)						
Compounds	**Class.I**	**Class.II**	**VIP**	**P-value**	**Fold Change**	**Type**
PA(21:0/i-15:0)	Lipids and lipid-like molecules	Glycerophospholipids	1.81	1.08E-05	0.32	Down
Penfluridol	Benzenoids	Benzene and substituted derivatives	1.81	9.73E-06	0.25	Down
PC(14:0/22:2(13Z,16Z))	Lipids and lipid-like molecules	Glycerophospholipids	1.79	3.86E-06	6.22	Up
Formetanate	Benzenoids	Benzene and substituted derivatives	1.79	1.31E-05	0.34	Down
Hydroxyzine	Benzenoids	Benzene and substituted derivatives	1.79	8.39E-05	2.10	Up
TG(18:2(9Z,12Z)/20:5(5Z,8Z,11Z,14Z,17Z)/18:4(6Z,9Z,12Z,15Z))	Lipids and lipid-like molecules	Glycerolipids	1.78	4.09E-06	0.22	Down
2-Amino-3-(3-methylbut-2-enylthio)propionic acid	Organic acids and derivatives	Carboxylic acids and derivatives	1.77	5.56E-05	0.37	Down
2-Methylamino-1-(3,4-methylenedioxyphenyl)butan-1-one	Benzenoids	Benzene and substituted derivatives	1.77	3.04E-05	0.44	Down
PA(i-21:0/a-15:0)	Lipids and lipid-like molecules	Glycerophospholipids	1.77	5.29E-05	0.42	Down
N-Formyldemecolcine	Hydrocarbon derivatives	Tropones	1.77	7.65E-05	0.32	Down
DG(22:1(13Z)/20:5(5Z,8Z,11Z,14Z,17Z)/0:0)	Lipids and lipid-like molecules	Glycerolipids	1.76	4.88E-05	5.45	Up
Bisphenol A diglycidyl ether	Benzenoids	Benzene and substituted derivatives	1.74	0.0002	0.36	Down
Medroxyprogesterone 17-acetate	Lipids and lipid-like molecules	Steroids and steroid derivatives	1.74	6.49E-05	0.42	Down
P-Aminohippuric Acid	Amino acid and Its metabolomics	Amino acid derivatives	1.74	0.0003	0.37	Down
Methylprednisolone succinate	Lipids and lipid-like molecules	Steroids and steroid derivatives	1.74	0.0005	0.28	Down
Gly Leu Arg Val Phe	–	–	1.74	1.27E-05	0.49	Down
N,N-Diethyl-3-methylbenzamide	Benzenoids	Benzene and substituted derivatives	1.74	5.07E-05	0.43	Down
Palustrine	Phenylpropanoids and polyketides	Macrolactams	1.74	0.0002	0.36	Down
PE-NMe2(20:5(5Z,8Z,11Z,14Z,17Z)/22:6(4Z,7Z,10Z,13Z,16Z,19Z))	Lipids and lipid-like molecules	Glycerophospholipids	1.73	0.0003	0.46	down
Coumarin-suberoylanilide hydroxamic acid	Phenylpropanoids and polyketides	Coumarins and derivatives	1.73	0.0001	0.41	down
Negative ion (ESI-)						
Compounds	**Class.I**	**Class.II**	**VIP**	**p_value**	**Fold_Change**	**Type**
cis-7,10,13,16,19-Docosapentaenoic acid	Lipids and lipid-like molecules	Fatty Acyls (脂肪酰类)	1.76	2.92E-05	2.47	Up
3,3'-Bisjuglone	Benzenoids	Naphthalenes	1.74	3.84E-05	0.40	Down
Prunasin	Alkaloids	Alkaloids	1.74	3.01E-05	0.40	Down
Raltitrexed	Organic acids and derivatives	Carboxylic acids and derivatives	1.72	9.94E-05	0.36	Down
L-Pipecolic acid	–	–	1.72	0.0006	0.39	Down
Lys Thr Gln Lys	–	–	1.72	0.0003	2.36	Up
Ziprasidone	Organoheterocyclic compounds	Diazinanes	1.71	2.54E-05	0.44	Down
Psoralen	Lignans and Coumarins	Coumarins	1.71	5.25E-05	0.42	Down
2-Arachidonyl Glycerol ether	Lipids and lipid-like molecules	Endocannabinoids	1.71	0.0001	0.36	Down
Artomunoxanthentrione	Organoheterocyclic compounds	Benzopyrans	1.71	9.25E-05	0.40	Down
Uridine	Nucleotide And Its metabolomics	Nucleotide and Its metabolomics	1.71	5.71E-05	2.63	Up
Decarboxy-Norlobaric Acid	Phenylpropanoids and polyketides	Depsides and depsidones	1.71	0.0001	0.41	Down
Chlorobenzene	Benzenoids	Benzene and substituted derivatives	1.70	0.0001	0.44	Down
Estradiol-17 3-sulfate	–	–	1.69	0.0001	0.40	Down
1-Oleoyl-sn-glycero-3-phosphocholine	-	-	1.69	0.0003	0.19	Down
11-deoxy-PGF1	Lipids and lipid-like molecules	Fatty Acyls	1.68	9.25E-05	0.47	Down
Thr Arg Lys Glu	–	–	1.68	0.0002	0.43	Down
1-Aminocyclohexanoic acid	Organic acid And Its derivatives	Organicacid and Its derivatives	1.68	0.0002	0.48	Down
Dattelic acid	Phenylpropanoids and polyketides	Cinnamic acids and derivatives	1.68	0.0002	0.41	Down
5'-Methoxyhydnocarpin-D	Lignans, neolignans and related compounds	Flavonolignans	1.67	0.0002	0.44	Down

Based on the differential metabolites, the Kyoto Encyclopedia of Genes and Genomes (KEGG) enrichment analysis was conducted. The path analysis results are shown in Figure 5 and Table 2, where we have selected the top 20 pathways in the positive ion mode and the negative ion mode. Previous studies have suggested that the changes in tryptophan

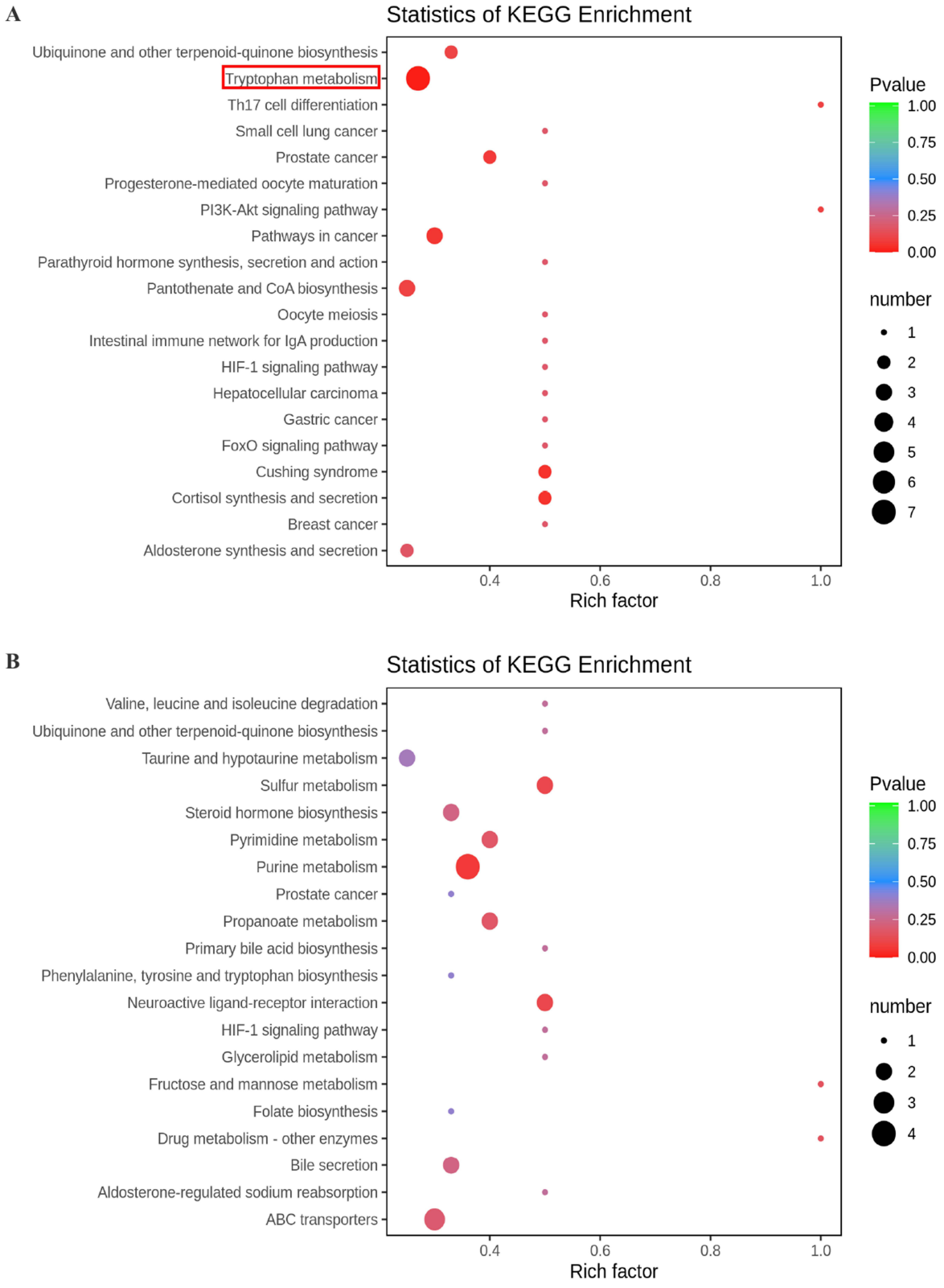

Figure 5 KEGG pathway enrichment analysis of differential metabolites between the control group and *Pneumocystis*-infected WT mice. (**A**) Positive and (**B**) negative ion modes.

Table 2 Pathway Enrichment Analysis of the Identified Metabolites Showing a Difference Between the Control Group and *Pneumocystis*-Infected WT Group Under ESI- and ESI+ Modes

Positive Ion (ESI+)		Negative Ion (ESI-)	
#Kegg_Pathway	**P-value**	**#Kegg_Pathway**	**P-value**
Tryptophan metabolism	0.0062	Purine metabolism	0.0682
Cortisol synthesis and secretion	0.0447	Sulfur metabolism	0.1128
Cushing syndrome	0.0447	Neuroactive ligand-receptor interaction	0.1128
Pathways in cancer	0.0562	Drug metabolism - other enzymes	0.1544
Prostate cancer	0.0701	Fructose and mannose metabolism	0.1544
Pantothenate and CoA biosynthesis	0.0903	Pyrimidine metabolism	0.1704
Th17 cell differentiation	0.0927	Propanoate metabolism	0.1704
PI3K-Akt signaling pathway	0.0927	ABC transporters	0.1855
Ubiquinone and other terpenoid-quinone biosynthesis	0.0990	Bile secretion	0.2319
Aldosterone synthesis and secretion	0.1643	Steroid hormone biosynthesis	0.2319
Parathyroid hormone synthesis, secretion and action	0.1769	Glycerolipid metabolism	0.2858
Progesterone-mediated oocyte maturation	0.1769	Ubiquinone and other terpenoid-quinone biosynthesis	0.2858
FoxO signaling pathway	0.1769	Valine, leucine and isoleucine degradation	0.2858
Small cell lung cancer	0.1769	HIF-1 signaling pathway	0.2858
Gastric cancer	0.1769	Aldosterone-regulated sodium reabsorption	0.2858
Hepatocellular carcinoma	0.1769	Primary bile acid biosynthesis	0.2858
Intestinal immune network for IgA production	0.1769	Taurine and hypotaurine metabolism	0.3575
HIF-1 signaling pathway	0.1769	Phenylalanine, tyrosine and tryptophan biosynthesis	0.3975
Oocyte meiosis	0.1769	Prostate cancer	0.3975
Breast cancer	0.1769	Folate biosynthesis	0.3975

metabolism play an important regulatory role in the host response during infection.[29] Our pathway enrichment analysis also showed that the tryptophan metabolism pathway was significantly enriched. We observed that some products of tryptophan metabolism were significantly changed in the lung samples of WT *Pneumocystis*-infected mice, including kynurenine, 4-(2-aminophenyl)-2,4-dioxobutanoic acid, 4,6-dihydroxyquinoline, N-acetyl-5-hydroxytryptamine. The pathway map of tryptophan metabolism is shown in Supplemental Figure 6.

To investigate why some products' levels of tryptophan metabolism were changed in the lung of WT *Pneumocystis*-infected mice, we measured the mRNA expression levels of key enzymes associated with the tryptophan metabolism in the lungs of control mice and *Pneumocystis*-infected WT mice. RT-PCR analysis showed that the mRNA level of indoleamine 2,3-dioxygenase 1(IDO1) and tryptophan hydroxylase (TPH) in the lungs was actually upregulated in *Pneumocystis*-infected WT mice (Figure 6). The results suggested that the tryptophan metabolism was activated and may play a potential role during *Pneumocystis* infection.

Lower Level of Alitretinoin and Abnormal Fatty Acid Metabolism in BAFF-R Gene Knockout *Pneumocystis*-Infected Mice

One hundred and five metabolites, mainly lipids and lipid-like molecules, were dysregulated (Supplemental Tables 4 and 5). Most of the differential metabolites of lipids and lipid-like molecules, such as farnesylthiosalicylic acid, PA (21:0/12:0), TG (14:0/18:1 (11Z)/18:1 (11Z)), PA (22:1 (13Z)/19:2 (10Z,13Z)), eicosapentaenoyl PAF C-16, PE-NMe (14:0/18:1 (11Z)), PC (18:1 (9Z)/22:2 (13Z,16Z)), alitretinoin, TG (16:0/14:1 (9Z)/20:3 (5Z,8Z,11Z)), and PE-Nme2 (15:0/16:0), were downregulation in BAFF-R–/– *Pneumocystis*-infected mice compared with WT *Pneumocystis*-infected mice (Supplemental Figure 7). The top 20 differential metabolites between the *Pneumocystis*-infected WT group and the *Pneumocystis*-infected BAFF-R$^{-/-}$ group with the highest VIP values under ESI- and ESI+ modes are shown in Table 3.

We next concentrated on metabolites and pathways involved in infection immunity and inflammation. Notably, the level of vitamin A's metabolite, alitretinoin, was lower in the lung samples of BAFF-R$^{-/-}$ *Pneumocystis*-infected mice than in WT *Pneumocystis*-infected mice. The KEGG enrichment analysis results are shown in Figure 7 and Table 4. The

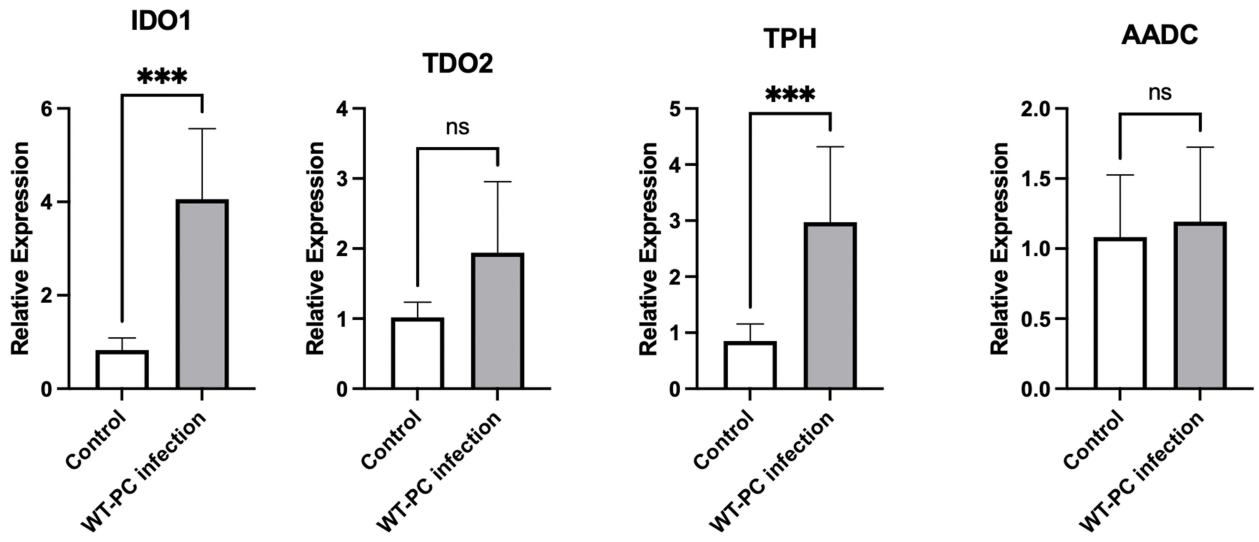

Figure 6 mRNA expression levels of enzymes associated with tryptophan metabolism in the lungs in the control group and *Pneumocystis*-infected WT mice (***P < 0.001).

analysis highlighted pathways related to fatty acid metabolism, such as the adipocytokine signaling pathway and fatty acid elongation. The pathway maps of the two pathways are presented in Supplemental Figures 8 and 9. Other studies have shown that fatty acid metabolism is related to infection immunity.[30]

We also measured the mRNA expression levels of enzymes associated with fatty acid metabolism in the lungs of the *Pneumocystis*-infected WT mice and *Pneumocystis*-infected BAFF-R$^{-/-}$ mice. The results of RT-PCR showed that the mRNA levels of stearoyl-CoA desaturase 1 (SCD1) and fatty acid synthase (FASN) in the lungs were significantly upregulated in BAFF-R$^{-/-}$ *Pneumocystis*-infected mice, and they both were positively correlated with the mRNA level of IL17A (Figure 8). The results revealed the metabolic dysregulation of fatty acid metabolism in BAFF-R$^{-/-}$ *Pneumocystis*-infected mice, possibly related to greater inflammatory cell infiltration in the lungs.

Discussion

Changes in the metabolic profile are the body's final response to stimuli. Untargeted metabolomics is an advanced way to screen unknown metabolite alterations. In recent years, metabolomics has been widely applied in infectious and immune diseases, and some metabolic changes have been found.[31–36] However, there is a lack of metabolomic information on *Pneumocystis* infection.

We found that many metabolites in WT *Pneumocystis*-infected mice were changed compared with non-infected mice. Lipids and lipid-like molecules were the primary dysregulated metabolites, indicating that lipid metabolism may be abnormal in *Pneumocystis* infection. Lipids have three main functions, namely, storing energy, forming an important component of cell membranes, and acting as important signaling molecules within cells. Many recent studies have explored lipid metabolism in diseases. As for infectious diseases, some studies have found lipid metabolism dysregulation in patients with COVID-19 or Mycoplasma *pneumoniae* pneumonia.[32,37] Our previous studies have suggested that B-cell counts are reduced after *Pneumocystis* infection,[18] and corticosteroid treatment might suppress the B-cell immunity in the PCP hosts.[15] Recent studies have shown that B-cell development and function are related to lipid metabolism.[38,39] Thus, correcting lipid metabolism disorders is a possible therapeutic target that may help promote B-cell function against *Pneumocystis* infection.

The current study focused on enriched metabolic pathways associated with anti-infection immunity. We noted significant changes in some metabolites associated with the tryptophan metabolism pathway during *Pneumocystis* infection. We also found that the expression levels of key enzymes of tryptophan metabolism, such as IDO1, was significantly upregulated. Many studies have revealed the role of tryptophan metabolism in regulating immune response.[40–42] In antitumor immunity, the activation of IDO1 may restrain antitumor immune responses by inhibiting

Table 3 Top 20 Differential Metabolites Between the *Pneumocystis*-Infected WT Group and *Pneumocystis*-Infected BAFF-R$^{-/-}$ Group with the Highest VIP Values Under ESI- and ESI+ Modes

Positive ion (ESI+)						
Compounds	**Class.I**	**Class.II**	**VIP**	**P-value**	**Fold Change**	**Type**
Lobaric acid	Phenylpropanoids and polyketides	Depsides and depsidones	2.32	0.0002	0.24	Down
Aldehydo-D-galactose	Organic oxygen compounds	Organooxygen compounds	2.26	1.50E-05	0.45	Down
DL-2-Aminocaprylic acid	–	–	2.24	0.0004	2.34	Up
Farnesylthiosalicylic acid	Lipids and lipid-like molecules	Prenol lipids	2.24	0.0005	0.29	Down
Isopropamide	Benzenoids	Benzene and substituted derivatives	2.18	7.36E-05	0.44	Down
N-3-Oxododecanoyl-L-homoserine lactone	Organic acids and derivatives	Carboxylic acids and derivatives	2.17	0.0010	0.23	Down
PA(21:0/12:0)	Lipids and lipid-like molecules	Glycerophospholipids	2.16	0.0008	0.46	Down
Taurodeoxycholate; Taurodeoxycholic acid	Lipids and lipid-like molecules	Steroids and steroid derivatives	2.15	0.0034	0.44	Down
TG(14:0/18:1(11Z)/18:1(11Z))	Lipids and lipid-like molecules	Glycerolipids	2.12	0.0059	0.37	Down
PA(22:1(13Z)/19:2(10Z,13Z))	Lipids and lipid-like molecules	Glycerophospholipids	2.10	0.0003	0.44	Down
Azelaic acid	–	–	2.10	0.0017	0.13	Down
Eicosapentaenoyl PAF C-16	Lipids and lipid-like molecules	Glycerophospholipids	2.06	0.0015	0.47	Down
1,24-Dihydroxyvitamin D3	Lipids and lipid-like molecules	Steroids and steroid derivatives	2.06	0.0064	7.52	Up
PE-NMe(14:0/18:1(11Z))	Lipids and lipid-like molecules	Glycerophospholipids	2.05	0.0045	0.44	Down
Carnitine C13:0	FA	CAR	2.03	0.0041	0.38	Down
PC(18:1(9Z)/22:2(13Z,16Z))	Lipids and lipid-like molecules	Glycerophospholipids	2.03	0.0052	0.47	Down
Alitretinoin	Lipids and lipid-like molecules	Prenol lipids	2.02	0.0015	0.49	Down
5-Hydroxytryptophol	Alkaloids	Plumerane	2.01	0.0026	0.38	Down
TG(16:0/14:1(9Z)/20:3(5Z,8Z,11Z))	Lipids and lipid-like molecules	Glycerolipids	2.01	0.0129	0.34	Down
PE-NMe2(15:0/16:0)	Lipids and lipid-like molecules	Glycerophospholipids	1.98	0.0006	0.34	Down
Negative ion (ESI-)						
Compounds	**Class.I**	**Class.II**	**VIP**	**p_value**	**Fold_Change**	**Type**
Hexanoyl Glycine	Amino acid and Its metabolomics	Amino acid derivatives	2.25	6.33E-05	0.20	Down
FFA(20:3)	Lipids	Free fatty acids	2.21	0.0009	0.49	Down
Sericetin	Phenylpropanoids and polyketides	Flavonoids	2.20	0.0014	0.41	Down
Lys Thr Gln Lys	–	–	2.17	0.0006	0.33	Down
Alpha-Bisabolol oxide C	Organoheterocyclic compounds	Oxanes	2.11	0.0011	0.14	Down
Phenethyl rutinoside	Organic oxygen compounds	Organooxygen compounds	2.10	0.0017	0.39	Down
Altanserin	Organic oxygen compounds	Organooxygen compounds	2.05	0.0031	0.40	Down
4-Hydroxybenzoic Acid	Phenolic acids	Phenolic acids	2.04	0.0024	0.34	Down
4-hydroxybenzenesulfonic acid	Organic acid And Its derivatives	Sulfonic acids	2.02	0.0030	0.33	Down
3-Sulfocatechol	Benzene and substituted derivatives	Phenolics	1.99	0.0006	0.39	Down
Phenol	Phenolic acids	Phenolic acids	1.99	0.0039	0.37	Down
cis-7,10,13,16,19-Docosapentaenoic acid	Lipids and lipid-like molecules	Fatty Acyls	1.97	0.0088	0.42	Down
2-Hydroxy-2-methylbutyric acid	Organic acids	Organic acids	1.81	0.0020	0.32	Down
Oleoylglycerone phosphate	Organic oxygen compounds	Organooxygen compounds	1.80	0.0186	2.33	Up
17α-Ethinylestradiol	Hormones and hormone related compunds	Hormones and hormone related compunds	1.67	0.0223	2.05	Up
Hydrocortisone acetate	Lipids and lipid-like molecules	Steroids and steroid derivatives	1.63	0.0084	0.43	Down
Adenosine 2'-Phosphate	Nucleotide And Its metabolomics	Nucleotide and Its metabolomics	1.60	0.0167	2.14	Up
4-Chloro-2-methylphenol	Benzenoids	Phenols	1.59	0.0150	2.39	Up
1-Oleoyl-sn-glycero -3-phosphocholine	-	-	1.59	0.0345	4.14	Up
Oleandolide	Phenylpropanoids and polyketides	Macrolides and analogues	1.51	0.0229	0.50	Down

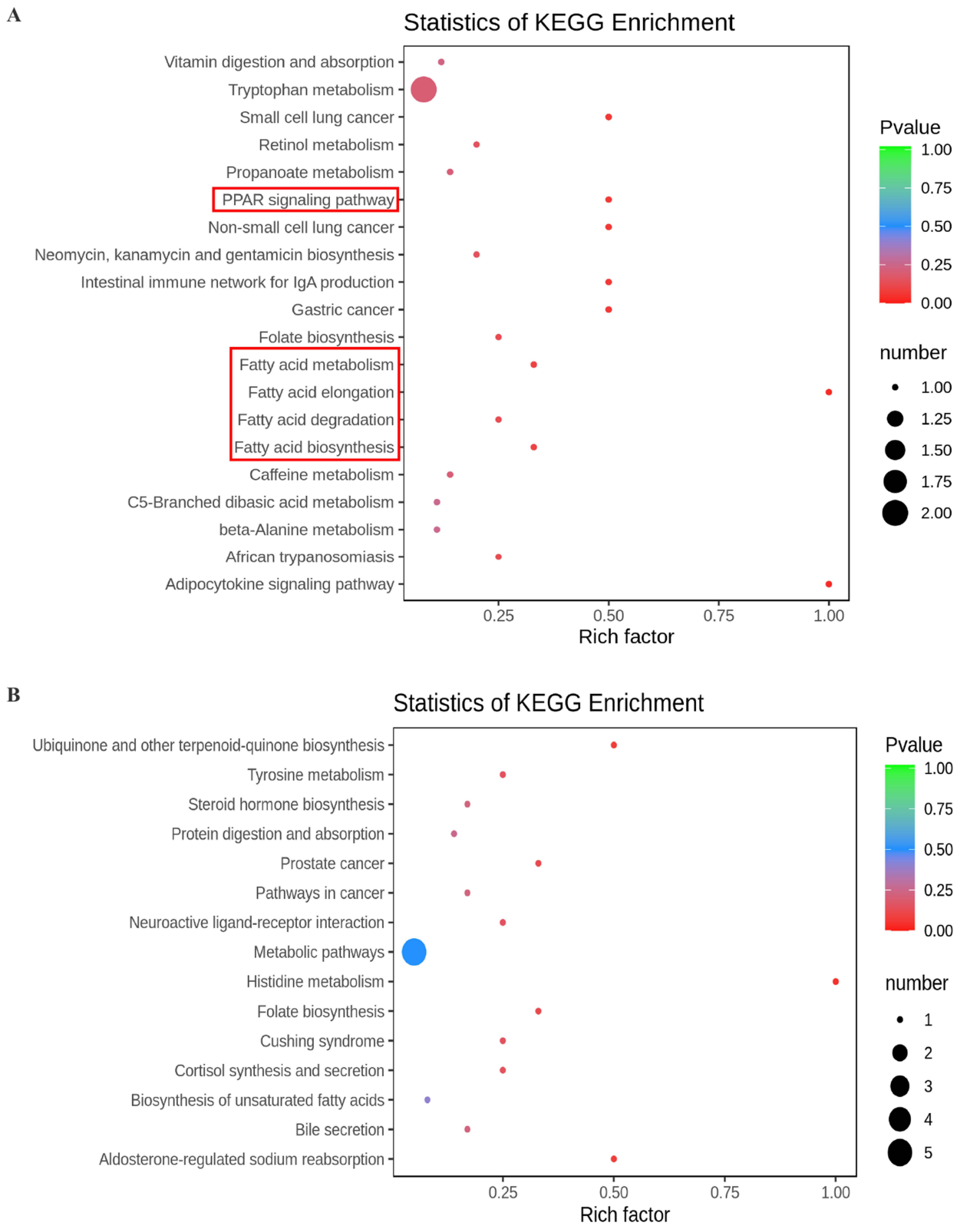

Figure 7 KEGG pathway enrichment analysis of differential metabolites between the *Pneumocystis*-infected WT mice and *Pneumocystis*-infected BAFF-R$^{-/-}$ mice. (**A**) Positive and (**B**) negative ion modes.

Table 4 Pathway Enrichment Analysis of the Identified Metabolites Showing a Difference Between the *Pneumocystis*-Infected WT Group and *Pneumocystis*-Infected BAFF-R$^{-/-}$ Group Under ESI- and ESI+ Modes

Positive Ion (ESI+)		**Negative Ion (ESI-)**	
#Kegg_Pathway	**P-value**	**#Kegg_Pathway**	**P-value**
Adipocytokine signaling pathway	0.0323	Histidine metabolism	0.0403
Fatty acid elongation	0.0323	Ubiquinone and other terpenoid-quinone biosynthesis	0.0792
Gastric cancer	0.0637	Aldosterone-regulated sodium reabsorption	0.0792
Small cell lung cancer	0.0637	Prostate cancer	0.1168
Non-small cell lung cancer	0.0637	Folate biosynthesis	0.1168
Intestinal immune network for IgA production	0.0637	Cortisol synthesis and secretion	0.1531
PPAR signaling pathway	0.0637	Cushing syndrome	0.1531
Fatty acid biosynthesis	0.0941	Neuroactive ligand-receptor interaction	0.1531
Fatty acid metabolism	0.0941	Tyrosine metabolism	0.1531
African trypanosomiasis	0.1236	Bile secretion	0.2219
Fatty acid degradation	0.1236	Steroid hormone biosynthesis	0.2219
Folate biosynthesis	0.1236	Pathways in cancer	0.2219
Retinol metabolism	0.1521	Protein digestion and absorption	0.2546
Neomycin, kanamycin and gentamicin biosynthesis	0.1521	Biosynthesis of unsaturated fatty acids	0.4012
Tryptophan metabolism	0.2027	Metabolic pathways	0.5038
Caffeine metabolism	0.2067		
Propanoate metabolism	0.2067		
Vitamin digestion and absorption	0.2327		
C5-Branched dibasic acid metabolism	0.2580		
Beta-Alanine metabolism	0.2580		

T cell function.[43] There is also evidence suggesting that tryptophan metabolism plays a vital role in infectious diseases.[43] Activation of IDO1 in our study may lead to impaired T-cell immunity against *Pneumocystis* infection and possibly lead to immune tolerance. Similar to our findings, in fungal infections, a recent study showed that *P. brasiliensis* infection induces a vigorous IDO expression.[44] In addition, the main pathway of tryptophan catabolism metabolism is the kynurenine pathway mediated by the key enzyme IDO1.[40,45,46] Kynurenine is the main downstream product of the IDO1. However, our study showed that compared with control mice, the product of tryptophan metabolism, kynurenine, was downregulated in the lung of WT *Pneumocystis*-infected mice, although the expression level of IDO1 was upregulated. This was probably due to an increase in kynurenine's incoming but more pronounced outgoing route. Hence, the results suggested a potential role of tryptophan metabolism in *Pneumocystis* infection. Given the complexity of the body's anti-*Pneumocystis* immunity, the current results are speculative, and further mechanistic studies are needed to explore the role of tryptophan metabolism in *Pneumocystis* infection.

$CD4^+$ T cells are crucial in controlling *Pneumocystis* infection.[47] Increasing evidence suggests that B cells also play an essential role in *Pneumocystis* infection.[48,49] Our previous study[18] found that the counts of B cells in mouse peripheral blood and lung tissue decreased after *Pneumocystis* infection, suggesting the significance of B cells. We further found that the clearance of *Pneumocystis* was delayed in BAFF-R$^{-/-}$ mice. However, current studies focus on the cellular level. Although we have done some molecular mechanism studies, metabolism-related studies on PCP are still lacking. Metabolism plays a crucial role in regulating the body's response to infection. Our study showed that many metabolites in the lung samples were altered in *Pneumocystis*-infected mice. In addition, there were differences in metabolites involved in the fatty acid metabolism in the lungs between WT *Pneumocystis*-infected mice and BAFF-R$^{-/-}$ *Pneumocystis*-infected mice.

Similar to our previous study,[18] as for the uninfected mice, BAFF-R$^{-/-}$ mice exhibited mainly the absence of mature B cells and a reduced but not complete lack of total B cells. We also observed no statistically significant differences in appearance, body weight, growth, and development between uninfected BAFF-R$^{-/-}$ mice and WT mice, so we did not set the group of uninfected BAFF-R$^{-/-}$ mice in the metabolomic analysis. As for the infected mice, we found that BAFF-R

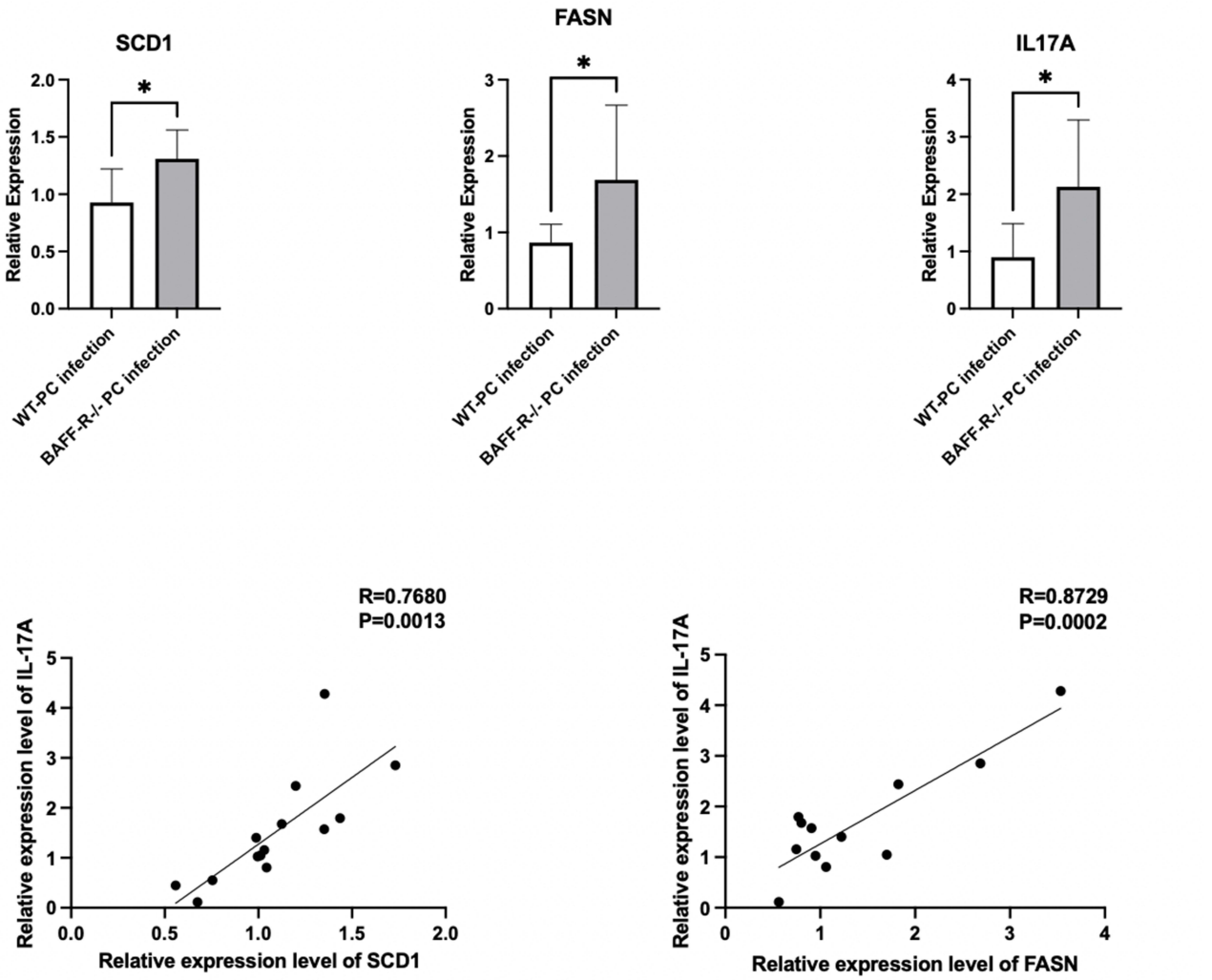

Figure 8 mRNA expression levels of enzymes associated with fatty acid metabolism in the lungs in the *Pneumocystis*-infected WT mice and *Pneumocystis*-infected BAFF-R$^{-/-}$ mice, and the correlation analysis of the mRNA expression levels of IL17A and SCD1 or FASN (*P < 0.05).

deficiency resulted in delayed clearance of *Pneumocystis* and more serious inflammatory cell infiltration in the lungs compared with *Pneumocystis*-infected WT mice in our previous study.[18] In comparing WT *Pneumocystis*-infected mice and BAFF-R$^{-/-}$ *Pneumocystis*-infected mice, we found some differential metabolites, mainly lipids and lipid-like molecules. For example, the level of vitamin A's metabolite, alitretinoin, was lower in the lung samples of BAFF-R$^{-/-}$ *Pneumocystis*-infected mice than in WT *Pneumocystis*-infected mice. Alitretinoin, also known as 9-cis-retinoic acid, is an isomer of all-trans retinoic acid.[50] As the active metabolites of vitamin A, much evidence has suggested that all-trans-retinoic acid and 9-cis-retinoic acid could increase the frequency of Treg cells and downregulate the frequency of Th17 cells.[51–53] It has been suggested that retinoic acid promotes the production of Tregs but restrains the differentiation of Th17 cells; it enhances the generation of Th2 but suppresses the Th1 cell differentiation of naïve T cells.[50] Furthermore, retinoic acid signaling is required for Th1 and Th17 immune responses to infection.[54] The lack of retinoic acid may enhance proinflammatory responses and diminish anti-inflammatory responses. It may be related to the recruitment of more inflammatory cells in the lung tissue of BAFF-R$^{-/-}$ mice. Although the recruitment of more inflammatory cells is intended to promote *Pneumocystis* clearance, excessive recruitment may lead to inflammatory damage, so more obvious alveolar hemorrhage was observed in the lung tissue of BAFF-R$^{-/-}$ mice.

We found some enriched metabolic pathways in BAFF-R$^{-/-}$ *Pneumocystis*-infected mice compared to WT *Pneumocystis*-infected mice, such as adipocytokine signaling pathway and fatty acid elongation. We also found

significantly increased expression of key enzymes of fatty acid metabolism, such as SCD1, FASN, in the lungs of BAFF-R$^{-/-}$ *Pneumocystis*-infected mice. Many studies have suggested that the significant expression increase of SCD1 and other key enzymes of fatty acid metabolism is associated with the dysregulation of proinflammatory genes.[55–57] This indicated a key role for fatty acid metabolism in regulating inflammation responses.

Our previous study demonstrated a significant role of B cells in defense against *Pneumocystis* infection.[15] Another study explored the role of B cells in regulating helper T lymphocytes' response to *Pneumocystis* infection[18] and suggested that BAFF-R deficiency prompted Th17-cell immune responses during *Pneumocystis* infection. This study found that elevated expression of key enzymes of fatty acid metabolism, such as SCD1, was positively correlated with IL17A levels. The results indicated that the abnormal fatty acid metabolism might be associated with the increased Th17-cell immune responses. We hypothesize that the over-recruitment of Th17 cells, although intended to promote *Pneumocystis* clearance, also caused more obvious lung damage during *Pneumocystis* infection in BAFF-R gene knockout *Pneumocystis*-infected mice.

Our results suggested that the metabolites, alitretinoin, as well as the products of fatty acid metabolism, may influence the inflammatory responses in *Pneumocystis* infection. In BAFF-R$^{-/-}$ *Pneumocystis*-infected mice, the balance between anti- and pro-inflammatory responses was disrupted, resulting in increased inflammatory damage. In short, these findings indicated that an appropriate Th1/Th17 response may contribute to the clearance of *Pneumocystis*, but an excessive response may result in inflammatory damage, where the balance between anti- and pro-inflammatory immunity is critical.

Overall, our study revealed the metabolic changes in the lungs of mice with *Pneumocystis* infection. However, there are some limitations to the study. First, the results of this study were based on the mouse model with limited sample sizes and lacked validation in PCP patients. Second, we only chose to observe the change of metabolites at a time point when the *Pneumocystis* burden was relatively high instead of observing the dynamic change of metabolites during the whole progression of *Pneumocystis* infection. Last but not least, future studies should be conducted to further explore the mechanism of metabolic changes.

Conclusions

In conclusion, many lipids and lipid-like molecules are dysregulated in *Pneumocystis* infection, which may influence B-cell development and function. The results also show noticeable changes in tryptophan metabolism in mice with *Pneumocystis* infection. In addition, the metabolomics analysis of the lung revealed a lower level of alitretinoin and the abnormality of fatty acid metabolism in BAFF-R gene knockout *Pneumocystis*-infected mice as compared with the WT *Pneumocystis*-infected mice, which may be related to the greater inflammatory cell infiltration in the lungs of BAFF-R$^{-/-}$ *Pneumocystis*-infected mice. The findings of metabolomic profiling of the lungs provide insights into developing novel therapeutic targets for PCP.

Abbreviations

PCP, Pneumocystis pneumonia; HIV, human immunodeficiency virus; BAFF-R, B cell-activating factor receptor; WT, wild-type; BAFF-R$^{-/-}$, BAFF-R deficient; ICU, Intensive care unit; TNF, tumor necrosis factor; SCID, severe combined immunodeficient; PCA, principal component analysis; OPLS-DA, orthogonal partial least squares discriminant analysis; VIP, variable importance in projection; FC, fold change; ESI+, electrospray ionization positive; ESI-, electrospray ionization negative; VAP, ventilator-associated pneumonia; CAP, community-acquired pneumonia; IDO1, indoleamine 2,3-dioxygenase 1; TPH, tryptophan hydroxylase; SCD1, stearoyl-CoA desaturase 1; FASN, fatty acid synthase.

Ethics Statement

The animal study was approved by Beijing Chao Yang Hospital, Capital Medical University. No. AEEI-2020-121.

Funding

This work was funded by the National Natural Science Foundation of China (No. 82270009) and the Natural Science Foundation of Capital Medical University (PYZ21084).

Disclosure

These authors report no conflicts of interest in this work.

References

1. Grønseth S, Rogne T, Hannula R, Åsvold BO, Afset JE, Damås JK. Epidemiological and clinical characteristics of immunocompromised patients infected with Pneumocystis jirovecii in a twelve-year retrospective study from Norway. *BMC Infect Dis*. 2021;21(1):659. doi:10.1186/s12879-021-06144-1
2. Cillóniz C, Dominedò C, Álvarez-Martínez MJ, et al. Pneumocystis pneumonia in the twenty-first century: HIV-infected versus HIV-uninfected patients. *Expert Rev Anti Infect Ther*. 2019;17(10):787–801. doi:10.1080/14787210.2019.1671823
3. Roux A, Canet E, Valade S, et al. Pneumocystis jirovecii pneumonia in patients with or without AIDS, France. *Emerg Infect Dis*. 2014;20(9):1490–1497. doi:10.3201/eid2009.131668
4. Enomoto T, Azuma A, Kohno A, et al. Differences in the clinical characteristics of Pneumocystis jirovecii pneumonia in immunocompromized patients with and without HIV infection. *Respirology*. 2010;15(1):126–131. doi:10.1111/j.1440-1843.2009.01660.x
5. Gingerich AD, Norris KA, Mousa JJ. Pneumocystis pneumonia: immunity, vaccines, and treatments. *Pathogens*. 2021;10(2). doi:10.3390/pathogens10020236
6. Shellito J, Suzara VV, Blumenfeld W, Beck JM, Steger HJ, Ermak TH. A new model of Pneumocystis carinii infection in mice selectively depleted of helper T lymphocytes. *J Clin Invest*. 1990;85(5):1686–1693. doi:10.1172/jci114621
7. Beck JM, Warnock ML, Curtis JL, et al. Inflammatory responses to Pneumocystis carinii in mice selectively depleted of helper T lymphocytes. *Am J Respir Cell Mol Biol*. 1991;5(2):186–197. doi:10.1165/ajrcmb/5.2.186
8. Fishman JA. Pneumocystis jiroveci. *Semin Respir Crit Care Med*. 2020;41(1):141–157. doi:10.1055/s-0039-3399559
9. Garvy BA, Wiley JA, Gigliotti F, Harmsen AG. Protection against Pneumocystis carinii pneumonia by antibodies generated from either T helper 1 or T helper 2 responses. *Infect Immun*. 1997;65(12):5052–5056. doi:10.1128/iai.65.12.5052-5056.1997
10. Hu T, Takamoto M, Hida S, Tagawa Y, Sugane K. IFN-γ deficiency worsen Pneumocystis pneumonia with Th17 development in nude mice. *Immunol Lett*. 2009;127(1):55–59. doi:10.1016/j.imlet.2009.08.013
11. Otieno-Odhiambo P, Wasserman S, Hoving JC. The contribution of host cells to pneumocystis immunity: an update. *Pathogens*. 2019;8(2):52. doi:10.3390/pathogens8020052
12. Kolls JK. An emerging role of B cell immunity in susceptibility to pneumocystis pneumonia. *Am J Respir Cell Mol Biol*. 2017;56(3):279–280. doi:10.1165/rcmb.2016-0360ED
13. Elsegeiny W, Eddens T, Chen K, Kolls JK, Deepe GS. Anti-CD20 antibody therapy and susceptibility to Pneumocystis pneumonia. *Infect Immun*. 2015;83(5):2043–2052. doi:10.1128/iai.03099-14
14. Opata MM, Hollifield ML, Lund FE, et al. B lymphocytes are required during the early priming of CD4+ T cells for clearance of pneumocystis infection in mice. *J Immunol*. 2015;195(2):611–620. doi:10.4049/jimmunol.1500112
15. Hu Y, Wang D, Zhai K, Tong Z. Transcriptomic analysis reveals significant B lymphocyte suppression in corticosteroid-treated hosts with pneumocystis pneumonia. *Am J Respir Cell Mol Biol*. 2017;56(3):322–331. doi:10.1165/rcmb.2015-0356OC
16. Mackay F, Schneider P, Rennert P, Browning J. BAFF AND April: a tutorial on B cell survival. *Annu Rev Immunol*. 2003;21(1):231–264. doi:10.1146/annurev.immunol.21.120601.141152
17. Thompson JS, Bixler SA, Qian F, et al. BAFF-R, a newly identified TNF receptor that specifically interacts with BAFF. *Science*. 2001;293(5537):2108–2111. doi:10.1126/science.1061965
18. Rong H-M, Li T, Zhang C, et al. IL-10-producing B cells regulate Th1/Th17-cell immune responses in Pneumocystis pneumonia. *Am J Physiol Lung Cell Mol Physiol*. 2019;316(1):L291–l301. doi:10.1152/ajplung.00210.2018
19. Jung J, Zeng H, Horng T. Metabolism as a guiding force for immunity. *Nat Cell Biol*. 2019;21(1):85–93. doi:10.1038/s41556-018-0217-x
20. Loftus RM, Finlay DK. Immunometabolism: cellular metabolism turns immune regulator. *J Biol Chem*. 2016;291(1):1–10. doi:10.1074/jbc.R115.693903
21. Rahman AN, Liu J, Mujib S, et al. Elevated glycolysis imparts functional ability to CD8(+) T cells in HIV infection. *Life Sci Alliance*. 2021;4(11). doi:10.26508/lsa.202101081
22. Jing Y, Luo L, Chen Y, et al. SARS-CoV-2 infection causes immunodeficiency in recovered patients by downregulating CD19 expression in B cells via enhancing B-cell metabolism. *Signal Transduct Target Ther*. 2021;6(1):345. doi:10.1038/s41392-021-00749-3
23. Gertsman I, Barshop BA. Promises and pitfalls of untargeted metabolomics. *J Inherit Metab Dis*. 2018;41(3):355–366. doi:10.1007/s10545-017-0130-7
24. Thomas T, Stefanoni D, Reisz JA, et al. COVID-19 infection alters kynurenine and fatty acid metabolism, correlating with IL-6 levels and renal status. *JCI Insight*. 2020;5(14). doi:10.1172/jci.insight.140327
25. Ceballos FC, Virseda-Berdices A, Resino S, et al. Metabolic profiling at COVID-19 onset shows disease severity and sex-specific dysregulation. *Front Immunol*. 2022;13:925558. doi:10.3389/fimmu.2022.925558
26. Xu J, Zhou M, Luo P, et al. Plasma metabolomic profiling of patients recovered from coronavirus disease 2019 (COVID-19) with pulmonary sequelae 3 months after discharge. *Clin Infect Dis*. 2021;73(12):2228–2239. doi:10.1093/cid/ciab147
27. Antcliffe D, Jiménez B, Veselkov K, Holmes E, Gordon AC. Metabolic profiling in patients with pneumonia on intensive care. *EBioMedicine*. 2017;18:244–253. doi:10.1016/j.ebiom.2017.03.034
28. den Hartog I, Zwep LB, Vestjens SMT, et al. Metabolomic profiling of microbial disease etiology in community-acquired pneumonia. *PLoS One*. 2021;16(6):e0252378. doi:10.1371/journal.pone.0252378
29. Schmidt SV, Schultze JL. New insights into IDO biology in bacterial and viral infections. *Front Immunol*. 2014;5:384. doi:10.3389/fimmu.2014.00384
30. Zhou X, Zhu X, Zeng H. Fatty acid metabolism in adaptive immunity. *Febs J*. 2021. doi:10.1111/febs.16296
31. Hussain H, Vutipongsatorn K, Jiménez B, Antcliffe DB. Patient stratification in sepsis: using metabolomics to detect clinical phenotypes, sub-phenotypes and therapeutic response. *Metabolites*. 2022;12(5). doi:10.3390/metabo12050376

32. Li J, Luu LDW, Wang X, et al. Metabolomic analysis reveals potential biomarkers and the underlying pathogenesis involved in Mycoplasma pneumoniae pneumonia. *Emerg Microbes Infect*. 2022;11(1):593–605. doi:10.1080/22221751.2022.2036582
33. Adu-Gyamfi CG, Snyman T, Hoffmann CJ, et al. Plasma indoleamine 2, 3-dioxygenase, a biomarker for tuberculosis in human immunodeficiency virus-infected patients. *Clin Infect Dis*. 2017;65(8):1356–1358. doi:10.1093/cid/cix550
34. Dewulf JP, Martin M, Marie S, et al. Urine metabolomics links dysregulation of the tryptophan-kynurenine pathway to inflammation and severity of COVID-19. *Sci Rep*. 2022;12(1):9959. doi:10.1038/s41598-022-14292-w
35. Zardini Buzatto A, Sarkar I, van Drunen Littel-van den Hurk S, Li L. Comprehensive Lipidomic and metabolomic analysis for studying metabolic changes in lung tissue induced by a vaccine against respiratory syncytial virus. *ACS Infect Dis*. 2020;6(8):2130–2142. doi:10.1021/acsinfecdis.0c00210
36. Zahoor I, Suhail H, Datta I, et al. Blood-based untargeted metabolomics in relapsing-remitting multiple sclerosis revealed the testable therapeutic target. *Proc Natl Acad Sci U S A*. 2022;119(25):e2123265119. doi:10.1073/pnas.2123265119
37. Hao Y, Zhang Z, Feng G, et al. Distinct lipid metabolic dysregulation in asymptomatic COVID-19. *iScience*. 2021;24(9):102974. doi:10.1016/j.isci.2021.102974
38. Weisel FJ, Mullett SJ, Elsner RA, et al. Germinal center B cells selectively oxidize fatty acids for energy while conducting minimal glycolysis. *Nat Immunol*. 2020;21(3):331–342. doi:10.1038/s41590-020-0598-4
39. Zhou X, Zhu X, Li C, et al. Stearoyl-CoA desaturase-mediated monounsaturated fatty acid availability supports humoral immunity. *Cell Rep*. 2021;34(1):108601. doi:10.1016/j.celrep.2020.108601
40. Dagenais-Lussier X, Loucif H, Beji C, Telittchenko R, Routy JP, van Grevenynghe J. Latest developments in tryptophan metabolism: understanding its role in B cell immunity. *Cytokine Growth Factor Rev*. 2021;59:111–117. doi:10.1016/j.cytogfr.2021.02.003
41. Grohmann U, Bronte V. Control of immune response by amino acid metabolism. *Immunol Rev*. 2010;236:243–264. doi:10.1111/j.1600-065X.2010.00915.x
42. Munn DH, Mellor AL. Indoleamine 2,3 dioxygenase and metabolic control of immune responses. *Trends Immunol*. 2013;34(3):137–143. doi:10.1016/j.it.2012.10.001
43. Platten M, Nollen EAA, Röhrig UF, Fallarino F, Opitz CA. Tryptophan metabolism as a common therapeutic target in cancer, neurodegeneration and beyond. *Nat Rev Drug Discov*. 2019;18(5):379–401. doi:10.1038/s41573-019-0016-5
44. de Araújo EF, Loures FV, Preite NW, et al. AhR ligands modulate the differentiation of innate lymphoid cells and T Helper cell subsets that control the severity of a pulmonary fungal infection. *Front Immunol*. 2021;12:630938. doi:10.3389/fimmu.2021.630938
45. Peyraud F, Guegan JP, Bodet D, Cousin S, Bessede A, Italiano A. Targeting tryptophan catabolism in cancer immunotherapy era: challenges and perspectives. *Front Immunol*. 2022;13:807271. doi:10.3389/fimmu.2022.807271
46. Moffett JR, Namboodiri MA. Tryptophan and the immune response. *Immunol Cell Biol*. 2003;81(4):247–265. doi:10.1046/j.1440-1711.2003.t01-1-01177.x
47. Morris A, Norris KA. Colonization by Pneumocystis jirovecii and its role in disease. *Clin Microbiol Rev*. 2012;25(2):297–317. doi:10.1128/cmr.00013-12
48. Lund FE, Schuer K, Hollifield M, Randall TD, Garvy BA. Clearance of Pneumocystis carinii in mice is dependent on B cells but not on P carinii-specific antibody. *J Immunol*. 2003;171(3):1423–1430. doi:10.4049/jimmunol.171.3.1423
49. Ruan S, Cai Y, Ramsay AJ, Welsh DA, Norris K, Shellito JE. B cell and antibody responses in mice induced by a putative cell surface peptidase of Pneumocystis murina protect against experimental infection. *Vaccine*. 2017;35(4):672–679. doi:10.1016/j.vaccine.2016.11.073
50. Larange A, Cheroutre H. Retinoic acid and retinoic acid receptors as pleiotropic modulators of the immune system. *Annu Rev Immunol*. 2016;34:369–394. doi:10.1146/annurev-immunol-041015-055427
51. Xiao S, Jin H, Korn T, et al. Retinoic acid increases Foxp3+ regulatory T cells and inhibits development of Th17 cells by enhancing TGF-beta-driven Smad3 signaling and inhibiting IL-6 and IL-23 receptor expression. *J Immunol*. 2008;181(4):2277–2284. doi:10.4049/jimmunol.181.4.2277
52. Abdolahi M, Yavari P, Honarvar NM, Bitarafan S, Mahmoudi M, Saboor-Yaraghi AA. Molecular mechanisms of the action of vitamin A in Th17/Treg axis in multiple sclerosis. *J Mol Neurosci*. 2015;57(4):605–613. doi:10.1007/s12031-015-0643-1
53. Mucida D, Park Y, Kim G, et al. Reciprocal TH17 and regulatory T cell differentiation mediated by retinoic acid. *Science*. 2007;317(5835):256–260. doi:10.1126/science.1145697
54. Hall JA, Cannons JL, Grainger JR, et al. Essential role for retinoic acid in the promotion of CD4(+) T cell effector responses via retinoic acid receptor alpha. *Immunity*. 2011;34(3):435–447. doi:10.1016/j.immuni.2011.03.003
55. Guo R, Xu X, Babcock SA, Zhang Y, Ren J. Aldehyde dedydrogenase-2 plays a beneficial role in ameliorating chronic alcohol-induced hepatic steatosis and inflammation through regulation of autophagy. *J Hepatol*. 2015;62(3):647–656. doi:10.1016/j.jhep.2014.10.009
56. Fang R, Yang S, Gu X, Li C, Bi N, Wang HL. Early-life exposure to bisphenol A induces dysregulation of lipid homeostasis by the upregulation of SCD1 in male mice. *Environ Pollut*. 2022;304:119201. doi:10.1016/j.envpol.2022.119201
57. Zhou J, Zhang N, Aldhahrani A, Soliman MM, Zhang L, Zhou F. Puerarin ameliorates nonalcoholic fatty liver in rats by regulating hepatic lipid accumulation, oxidative stress, and inflammation. *Front Immunol*. 2022;13:956688. doi:10.3389/fimmu.2022.956688